Structure and elastic properties of Al-doped Mo/Ni superlattices

John L. Makous and Steven M. Hues
Surface Chemistry Branch, Naval Research Laboratory, Washington, D.C. 20375-5000
(Received 8 April 1991)

Undoped Mo/Ni superlattices have previously been shown to exhibit a softening of the c_{44} shear elastic constant with decreasing bilayer thickness. Using ion-beam sputtering, we deposited a series of Mo/Ni superlattice films doped with Al at various concentrations up to 25 at. %. We used Auger electron spectroscopy, x-ray photoelectron spectroscopy, and x-ray diffraction to characterize the chemical and structural properties of the films. The elastic properties of the films were characterized using an improved surface-acoustic-wave (SAW) technique for measuring SAW velocities. We also demonstrate that linear perturbation theory can be used to determine information about the elastic properties of thin films from SAW measurements. We find that the effect of the Al doping on the structural, chemical, and elastic properties of Mo/Ni is small at Al concentrations up to $\sim$15 at. %. From Auger bevel-map profiles we find that the Al is segregating to the Ni layers. The ability of the Mo/Ni system to tolerate this high concentration of Al is postulated to result from the formation of Ni_3Al, whose structural constants closely match those of Ni. At higher Al concentrations a breakdown of the superlattice structure is accompanied by a rehardening of the c_{44} stiffness constant.

I. INTRODUCTION

Studies concerning the elastic properties in layered systems may be traced back to 1937.[1] These initial calculations, which treat each layer as a medium with elastic constant c_{ij}, and the many generalizations that follow,[2] all show that the effective elastic constants of a composite system are given as averages of the moduli of the constituents. In addition, in the long-modulation-wavelength limit the elastic moduli are shown to be independent of the modulation wavelength, and depend only on the relative amounts of each material. The modulation wavelength Λ is defined as the thickness of one A/B bilayer in an alternating $A/B/A/B/A\ldots$ structure. Metallic superlattice films, on the other hand, have been shown to exhibit anomalous elastic properties as a function of modulation wavelength. The sense of these anomalies is system specific, but usually some sort of softening or hardening in the c_{44} shear elastic stiffness constant is observed at decreasing Λ below $\sim$50 Å. For a review of this effect, see Ref. 3.

An issue that has not been addressed is the effect of contaminants on the structural and elastic properties of metallic superlattices. Conceivably, this issue is especially important at small Λ, where interfaces dominate the structure. Sample contamination during preparation may result from several sources. The most common is from the adsorption of vacuum contaminant species (water, oxygen, hydrocarbons, etc.) onto the growing surface during film deposition. This is of particular concern in high-vacuum systems (i.e., base pressure $>10^{-7}$ Torr). However, even under ultrahigh-vacuum conditions (i.e., base pressure of 10^{-9}–10^{-11} Torr), where vapor-phase impurities are a minimum, contamination during film growth can come from the sputtering-target holder (typically aluminum, copper, or stainless steel) or other interior surfaces that may be sputtered or evaporated during deposition and become incorporated into the growing film. The question is at what level do contaminants begin to affect the structural and elastic properties of thin films and multilayers.

In this study the structural properties and shear elastic constant of a series of Mo/Ni superlattice films have been studied as a function of aluminum incorporation. The Mo/Ni system was chosen because it has previously been seen to exhibit a large ($\sim$44%) decrease in the c_{44} elastic stiffness constant as a function of decreasing modulation wavelength.[4] Aluminum was chosen as an impurity for several reasons. It is a common sputtering-target housing material and has been found in sputtered films on the 1% level.[5] Also we are interested in the possibility of artificially introducing strain into the films and examining the resulting structural and elastic effects. Previous work[4,6] has shown that the elastic properties of Mo/Ni are predominantly determined by the strain in the Ni lattice. However, Al can form a highly ordered intermetallic nickel aluminide compound, Ni_3Al, which has a fcc structure very similar to that of bulk nickel, where the lattice constant of Ni_3Al differs from that of bulk Ni by 1.5%.[7] Therefore, we are curious to see how Al is incorporated into the Mo/Ni multilayers, and how any resulting structural effects might alter the elastic properties of these films.

Multilayers of Mo/Ni, fabricated by ion-beam sputtering with modulation wavelengths in the $9 \leq \Lambda \leq 150$ Å regime, were doped with Al at various concentrations up to approximately 25 at. %. Their elastic properties were characterized by a surface-acoustic-wave (SAW) technique, which we describe here in detail. The chemical properties of these films were analyzed using Auger-electron spectroscopy (AES) and x-ray photoelectron spectroscopy (XPS), and their structures were character-

ized by x-ray diffraction (XRD). We have found that Al concentrations of up to approximately 15 at. % have very little effect on either the structural or elastic properties of Mo/Ni superlattices. Auger analyses indicate a strong segregation of the Al into the Ni layers, even though the Al was codeposited into both the Mo and Ni layers. At concentrations above 15 at. % noticeable effects on both the crystalline structure and elastic properties are observed. These concentration effects will be discussed here in detail.

II. SAMPLE PREPARATION

The Mo/Ni multilayered films were prepared by ion-beam sputtering in a cryopumped deposition chamber (Commonwealth Scientific) at typical base pressures of $(1-2)\times10^{-7}$ Torr. The ion energy and beam current of the Ar sputtering beam were 800 eV and 55 mA, respectively, while the partial pressure of 99.9995%-pure Ar during deposition was 3×10^{-4} Torr. The Mo and Ni targets, which are 99.95% pure, were mounted on a rotation stage from which the active sputtering target could be selected. Multilayered films were deposited by repeatedly alternating from the Mo target to the Ni target, with the ion-gun voltage shut off during rotation. Feedback control of the ion-beam current and computer control of the target sequencing enable constant ($\pm\sim0.5\%$) layer thicknesses during a deposition. The multilayers were deposited with equal Mo and Ni layer thicknesses at a rate of approximately 2 Å/s, and the temperature of the substrates, which include Si(100), bare ST-cut quartz, and masked ST-quartz SAW wafers, was not controlled during the deposition. Al was incorporated by cosputtering from Al targets placed over portions of the Mo and Ni targets. Using AES, the amount of Al incorporated into the films was quantified and varied by adjusting the size and position of the Al pieces of the targets.

III. ELASTIC PROPERTIES

The elastic properties of the Mo/Ni films were characterized using an improvement on the SAW technique described in Ref. 8. By measuring the time of flight (TOF) of a SAW propagating across a known substrate with a film overlay, one can determine information about the shear elastic properties of the overlay. Here we describe a method that enables the TOF of the SAW's to be measured easily and accurately, making this technique simple to use. Also, in interpreting the SAW velocity measurements we compare linear perturbation theory with the analysis described in Ref. 8, in which a simple analytical dependence of the SAW velocity on the film thickness is assumed. We find very good qualitative agreement between these data interpretations. Here we present in detail the methods used in measuring the SAW velocities and in analyzing the data.

A. SAW velocity measurements

The SAW device used in these measurements consists of an array of six aluminum transducers spaced at 4-mm intervals along the X-propagating direction of an ST-quartz wafer, as shown schematically in Fig. 1(a). The interdigital transducers were fabricated using standard photolithographic techniques and consist of 5-mm-long fingers that are 5 μm wide with 5-μm spacings. These interlaced fingers are arranged in a split-finger design, and the transducer geometry of our devices defines a fundamental acoustic wavelength of 40 μm, which corresponds to an operating frequency of 79 MHz.

The SAW velocity, $v(kh)$, across the film/substrate path is determined by the formula

$$v(kh)=(1/v_0+\Delta t/L)^{-1}\ , \tag{1}$$

where k is the wave vector of the SAW, h is the film thickness, v_0 is the SAW velocity of the substrate, Δt is the *change* in the TOF of the SAW across the film/substrate path due to the film, and L is the propagation length of the SAW across the film. For ST-cut quartz the open-circuit phase velocity is 3 158 m/s along the X axis;[9] however, since the metallic overlays are conducting, the short-circuit value of 3 156 m/s was used.[10]

The propagation length, L is defined by the mask used during the film-deposition process. The same shim stock mask was used for all of the films, where $L=2.4\pm0.025$ mm, as measured by a Tencor Alpha-Step profilometer

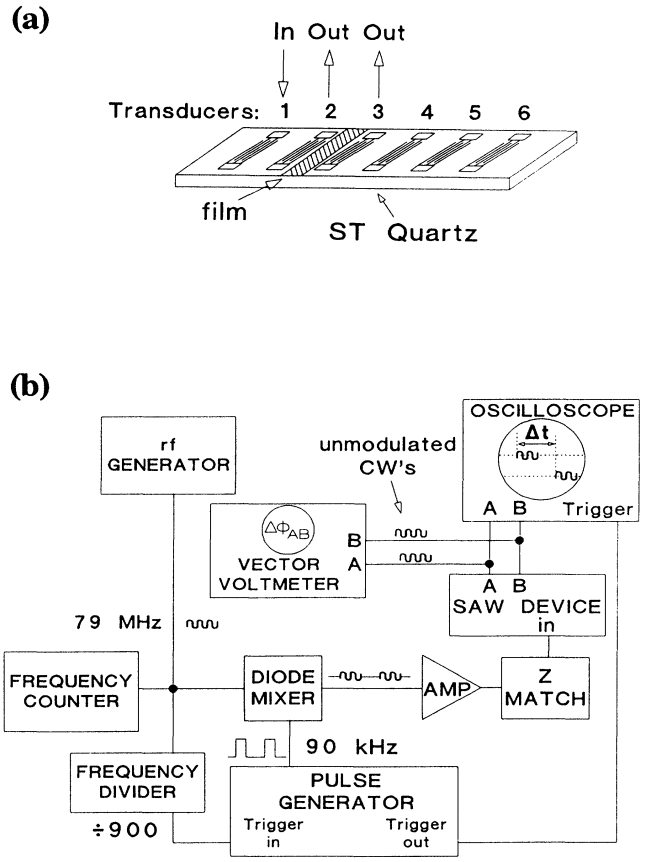

FIG. 1. (a) Schematic diagram of the SAW device. (b) Block diagram of the electronics used in the SAW measurements.

and an optical microscope.

The TOF of the SAW, τ, is determined to within a fraction of a nanosecond using a combination of techniques. The input signal is fed into one of the transducers on the substrate and the two output signals, taken at the transducers on either side of the film as indicated in Fig. 1(a), are compared in order to determine the relative TOF of the SAW between them. Comparing the TOF before and after film deposition yields the shift Δt. We use the period of the SAW, which is approximately 12.6 ns, to measure the TOF in the following way. The TOF, in general, will be a nonintegral number of SAW periods. The integral part is determined by measuring to within one SAW period an approximate value for the TOF, which is then divided by the SAW period to yield an integer plus a fraction. The fractional part is determined very precisely by a vector voltmeter, which interferometrically measures the relative phase between the outputs to within a fraction of a degree of the SAW wave period. The integral plus fractional parts are then combined to calculate the total time shift to within a fraction of a nanosecond.

One method of determining an approximate value of the TOF is based on the pulse method described in Ref. 8. The electronic setup for this method is shown in Fig. 1(b). A 79-MHz carrier-wave (CW) signal, whose frequency is determined by a Philips PM 6674 frequency counter, is generated by a Hewlett-Packard 608D VHF generator, and a 400-ns-wide pulse, generated at a frequency of 90 kHz by a Hewlett-Packard 1900A pulse generator, is used to modulate this CW via a diode mixer. An impedance-matching element is used between the diode mixer and the SAW device, and the modulated CW is fed into one of the transducers. The outputs are displayed on separate channels on the screen of a Tektronix 2465A oscilloscope, where the two output pulse envelopes are seen. Using the DELAY MODE on the oscilloscope, we can adjust the time delay between the signals on the oscilloscope screen until their envelopes exactly overlay. In this way the relative TOF of the SAW across the film may be determined. To keep all of the signals in phase and eliminate jitter on the oscilloscope screen, the oscilloscope is triggered by the pulse generator, which is triggered by a divided-down signal from the CW generator.

Because of the high frequency of the CW, it is difficult with this technique to determine exactly which periods of the CW's under the two output modulation envelopes overlay, i.e., the temporal definition of the modulation envelope is not easily defined within one CW period on the oscilloscope screen, which can result in an uncertainty in the TOF on the order of 12.6 ns. Therefore, we devised what we believe is a novel technique for determining the SAW TOF that takes advantage of the linear arrangement of the transducers on the substrate. The unmodulated CW is input into a transducer not adjacent to the film [e.g., 1 in Fig. 1(a)], the outputs are taken at the two transducers adjacent to the film [e.g., 2 and 3 in Fig. 1(a)], and their phases are compared on a Hewlett-Packard 8405A vector voltmeter. By varying the frequency of the signal around the 79-MHz fundamental of the device, we can determine the frequencies at which the two outputs are in phase. At these frequencies the path difference of the signal to the two outputs is equal to an integer number of SAW wavelengths. It can be shown that these frequencies are related to the relative TOF, τ, by the relation $M=\tau f_m$, where M is an integer, and f_M denotes the frequencies at which the outputs are in phase. The bandpass Δf of the transducers is related to the number of fingers in the transducer, N_t, by the relation $f_0/\Delta f=N_t$, f_0 being the fundamental frequency of the device.[11] In our devices $N_t=20$, and so $\Delta f\approx 4$ MHz at 79 MHz. The frequency interval at which the outputs are in phase is approximately 0.8 MHz or less, depending on whether or not the film is present. Therefore, by measuring several successive f_M we can determine τ to within a few nanoseconds.

This technique, complemented by the pulsed-envelope method, enables us to determine the number of integral cycles of the CW that make up the TOF. The vector voltmeter is used to pinpoint the TOF by measuring the phase difference between the outputs to within a fraction of a degree, which corresponds to a precision on the 10-ps level. The arrangement of the six transducers on the substrate enables us to make several TOF measurements by permutating which transducers are the input and the outputs, as long as the film is located somewhere between the outputs. We typically find the variance among several measurements with different input-output combinations to be on the order of 100–200 ps, which is taken as the uncertainty in the TOF measurements.

In summary, with the apparatus described above we are able to measure the TOF of a SAW with an accuracy of 100–200 ps. The geometry of our devices results in a TOF of approximately 1266 ns between adjacent transducers across the bare quartz, where each device is calibrated prior to the film deposition. A 5000-Å-thick Mo/Ni film typically will introduce a delay on the order of 20 ns.

B. SAW data analysis

The SAW amplitude displacements extend below the surface to distances on the order of the SAW wavelength, λ_s, where $\lambda_s=40\ \mu$m. Since our films are roughly 5000 Å thick, the substrate greatly influences the SAW velocity, and the films cause only slight shifts in the velocity. Therefore, in order to obtain information about the elastic properties of the film from the measured velocity $v(kh)$, we analyzed the SAW measurements using two methods. The first method, which was used previously by Danner *et al.*,[8] assumes the functional relation

$$v(kh)=v_f+(v_0-v_f)[1-\tanh(kh)]\ , \tag{2}$$

where v_f and v_0 are the phase velocities of an infinitely thick film and of the quartz substrate respectively. This function is used in place of solving the acoustic-wave equations and utilizing fitting routines, a process that would be necessary for each Λ and would require several measurements at different film thicknesses for each modulation wavelength.

As we demonstrate presently, the relative behavior of the film velocities determined by the method of Eq. (2) agrees qualitatively with linear perturbation theory, which is the second method we used for analyzing the SAW data. For a thin, isotropic, nonpiezoelectric overlay of thickness h on a substrate which has an unperturbed velocity v_0, the perturbed velocity $v(kh)$ can be written to first order as[12]

$$v(kh)=v_0-\tfrac{1}{4}\rho v_0^3\{(1-c_{44}/\rho v_0^2)P_x^2+P_y^2+[1-(1+c_{12}/c_{11})c_{44}/\rho v_0^2]P_z^2\}(kh)\ , \tag{3}$$

where ρ is the density of the film, the c_{ij} are the elastic stiffness constants of the film, and the P_i are the normalized particle velocity components at the surface. These are tabulated for many materials according to their crystalline orientation, and for ST quartz P_x is negligible compared to P_y and P_z.[9] Therefore, if the density of the film is known, one can determine the quantity $(1+c_{12}/c_{11})c_{44}/\rho v_0^2$ from the experimentally measured $v(kh)$. This quantity is proportional to v_f^2, where $v_f \approx (c_{44}/\rho)^{1/2}$.

To check this technique we measured a series of undoped, ~5000-Å-thick Mo/Ni superlattices with $27.7 \leq \Lambda \leq 143$ Å. The modulation wavelengths were determined from x-ray-diffraction spectra, which are discussed in detail below, and the exact values of the film thicknesses were taken as the product of Λ times the total number of deposited bilayers. These film thicknesses were verified by surface-profilometer measurements, and the results of both measurements were found to agree to within the precision of the profilometer (approximately ±10%). A density of 9.6 g/cm^3, which is an average of bulk Mo and Ni, was taken as the density of the films. The measured velocity shifts were analyzed by the two different methods discussed above; so for each film we have two elastic quantities: the phase velocity v_f from Eq. (2) and the elastic term $(1+c_{12}/c_{11})c_{44}/\rho v_0^2$ determined from linear perturbation theory, which are both plotted in Fig. 2 as a function of Λ.

A comparison of qualitative behavior of these two elastic quantities indicates excellent agreement, where both show a general decrease with decreasing Λ. This elastic softening agrees with the elastic behavior of Mo/Ni superlattices reported in Ref. 4, where the surface-wave velocities were determined by Brillouin light scattering. Therefore, we conclude that the SAW technique presented here is valid for comparing the relative elastic properties of thin films, in agreement with the findings reported in Ref. 8. From now on we will refer to the velocity v_f determined from Eq. (2) when comparing the measured elastic properties of the films.

In Fig. 3 the velocities of Mo/Ni multilayers doped

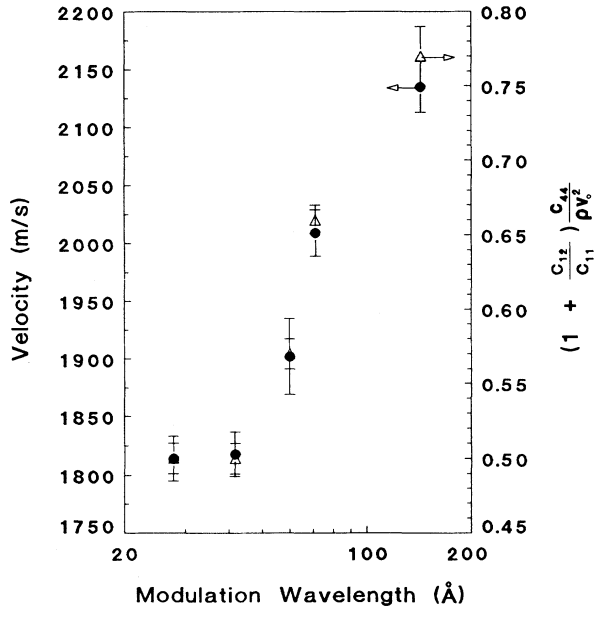

FIG. 2. Surface-wave velocities, v_f, (●), calculated from Eq. (2) and the elastic term $(1+c_{12}/c_{11})c_{44}/\rho v_0^2$ (△) determined by linear perturbation theory plotted as a function of Λ for undoped Mo/Ni superlattices.

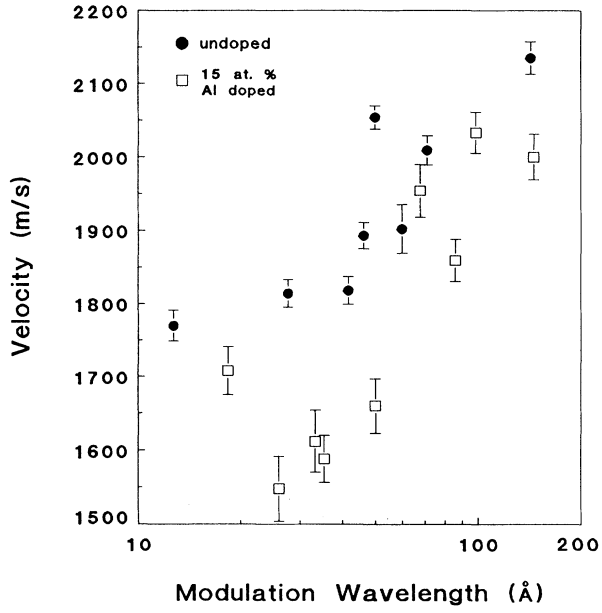

FIG. 3. Surface-wave velocities, v_f, of undoped (●) and 15 at. % Al-doped (□) Mo/Ni superlattices plotted as a function of Λ.

with approximately 15 at. % Al are plotted as a function of Λ along with the velocities of the undoped films represented in Fig. 2. Both velocity sets follow a similar softening trend with decreasing Λ, where the doped films show a slightly larger decrease in v_f. It seems that the addition of approximately 15 at. % Al does not greatly affect the shear elastic stiffness of Mo/Ni superlattices. In contrast, Mo/Ni films doped with approximately 20–25 at. % Al exhibit no elastic softening with decreasing Λ, as observed by the SAW measurements. Below we discuss the chemical and structural behavior of the Al-doped films and explain why no elastic effects are observed until dopant levels of approximately 20 at. % Al.

IV. CHEMICAL ANALYSIS

A Perkin-Elmer PHI 660 scanning Auger multiprobe was used to determine the chemical composition of the films and also to verify the chemical modulation of the layers. Analyses were performed using 5-keV primary electrons at a current of 0.34 μA and a base pressure of 5×10^{-10} Torr. Sputtering during depth profiling analysis was conducted with a 3 keV Ar^+ primary ion beam rastered over a 2×2-mm^2 area, and concentration scales were determined using the relative sensitivity factor method.[13] As the individual layer thicknesses were extremely thin (as low as 5 Å), the combined effects of atomic mixing and sputter-induced roughness[14] reduced the depth resolution of the sputter-depth profiles to the point where the individual layers in most samples could not be distinguished. Because of these effects, the Al concentration reported for a given film is the average Al concentration over the sputtered depth.

In Fig. 4 we show the Auger depth profile of a $\Lambda=98.6$ Å sample. As seen in this figure, there is a slight modulation in the Al concentration with depth, as was noticed in some of the longer-wavelength superlattices. In order to examine this further, a modification of the bevel-depth-profiling technique[15] was performed by producing Auger compositional maps of the walls of ion-beam-sputtered craters. In order to produce well-defined crater walls, the ion sputtering was performed in a Cameca IMS-3f ion microscope using an 8.0-keV (impact energy) Ar^+ beam focused to 25 μm^2 rastered over a 500×500-μm^2 area, resulting in a square crater. The samples were then transferred to the Auger vacuum chamber and lightly sputter cleaned until O and C signal levels achieved a steady state. As one approaches the top of the crater, the angle formed between the crater wall and the sample surface becomes more shallow, allowing one to change the apparent "magnification" of the image by selecting areas of different crater-wall angle.

The Auger compositional maps of Mo, Ni, and Al, determined from the bevel-depth profile (of the same sample as in Fig. 4), are shown in Fig. 5. Because we are looking at a corner of the crater, where the bevel is especially shallow, the mapped layers appear curved. Comparing the Mo, Ni, and Al maps in the figure, one sees that indeed there is a strong modulation in the Al con-

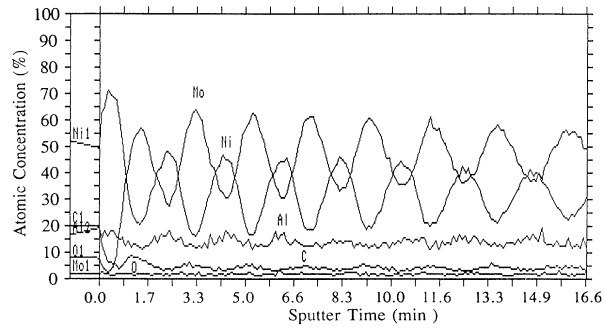

FIG. 4. Auger-depth profile showing atomic concentration vs sputtering times for a $\Lambda=98.6$ Å Mo/Ni superlattice doped with 15 at. % Al. The profiles of Mo, Ni, Al, O, and C are indicated.

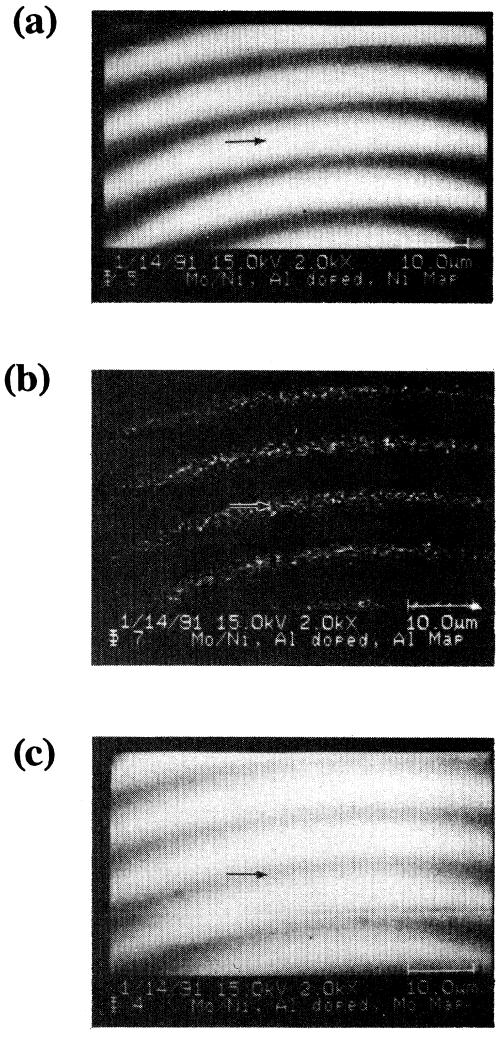

FIG. 5. AES compositional maps for (a) Ni, (b) Al, and (c) Mo in a $\Lambda=98.6$ Å Mo/Ni superlattice doped with 15 at. % Al. Light regions correspond to where the element is detected, and the arrows indicate the same position on the sample.

centration, in phase with the Ni layers. The Al appears to be localized in the Ni layers with the resulting concentration in the Mo layers being below the detection limit of the Auger analysis in the mapping mode (~ 1 at. %).

XPS was employed as an additional tool for probing the chemical nature of the Mo/Ni films. The samples were measured using a Surface Science Instruments SSX-100-03 small-spot system with monochromated Al $K\alpha$ radiation. The analyses were performed at a base pressure of $\sim 1\times 10^{-9}$ Torr, and the samples were sputter cleaned to remove the surface layer by rastering a 3-keV Ar^+ ion beam over a 3×3-mm^2 area for 5 min until the O and C signal intensities reached a steady-state level. We measured an undoped sample at $\Lambda=71$ Å, a sample doped with 15 at. % Al at $\Lambda=86$ Å, and a sample doped with approximately 25 at. % Al at $\Lambda=51$ Å. A comparison of the spectra for all three samples indicates no shifts in the binding energies nor any changes in the line shapes of the Ni $2p_{3/2}$ and the Mo $3d_{5/2}$ peaks, which were found at 853.0 and 227.9 eV, respectively, and correspond to the elemental metals.[16] In the 15 at. % Al–doped sample the Al $2p$ peak was found with a binding energy of 72.5 eV, again consistent with elemental Al.[16] However, for the 25 at. %–doped sample an additional peak at 74.4 eV was detected. This peak corresponds to oxidized Al, presumably Al_2O_3 (or possibly $NiAl_2O_4$).[17]

The findings from the XPS data indicate an increased Al-oxide content with increasing Al concentration in the films, where oxidized Al is detected only in the film doped with 25 at. % Al and not in the sample doped with 15 at. % Since Al has a very strong affinity for oxygen, we suspect that the oxidation is occurring in the XPS chamber during the analysis, even though the chamber was at $\sim 1\times 10^{-9}$ Torr. The other possibility is that the oxidation occurred during the deposition of the film. In either case the detection of Al-oxide in the 25 at. %–doped films and not the 15 at. %–doped films is most likely because there is more Al in the 25 at. %–doped film, where an aluminum oxide peak would be more noticeable.

V. STRUCTURAL CHARACTERIZATION

The structures of the films were characterized by x-ray diffraction using Cu $K\alpha$ radiation in a Rigaku θ-2θ Bragg-Brentano diffractometer with a rotating anode. Both high- and low-angle scans were performed to elucidate information about the superlattice structure and composition modulation of the films. In Fig. 6 the high-angle spectra of several undoped superlattices are shown with modulation wavelengths in the range $12.5\leq\Lambda\leq 143$ Å. These spectra, which correspond to the (111) reflections of Ni and the (110) reflection of Mo, demonstrate the expected superlattice behavior.[18] The x-ray peaks are reasonably sharp for $27.7\leq\Lambda\leq 143$ Å, signifying superlattice coherency over many layers in the perpendicular direction. Analysis of the full width at half maxima (FWHM's) of the Bragg peaks (at $2\theta\approx 42°$) using the Scherrer equation[19] indicates a roughly constant perpendicular structural coherence length of 150–200 Å for

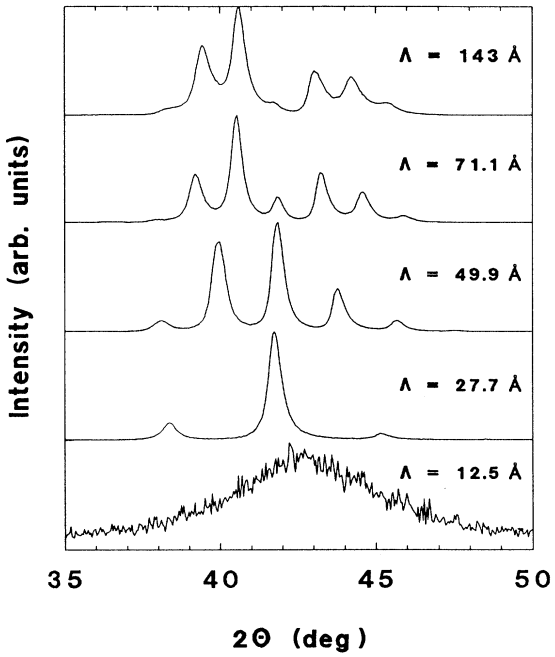

FIG. 6. High-angle x-ray-diffraction spectra for a series of undoped Mo/Ni superlattices.

$\Lambda\geq 27$ Å. In the $\Lambda=12.5$ Å spectrum the sharp x-ray peaks are replaced by one rather broad peak, indicating that a breakdown in the structural coherence occurs for Λ somewhere between 12.5 and 27.7 Å. This agrees with the structural behavior of the Mo/Ni films reported in Ref. 4, where a breakdown in the long-range crystalline order was observed for $\Lambda\leq 16.6$ Å.

The high-angle x-ray spectra of several Mo/Ni multilayers doped with 15 at. % Al are shown in Fig. 7 for $24.8\leq\Lambda\leq 98.6$ Å. These behave similarly to the undoped samples in Fig. 6, demonstrating sharp superlattice lines for $\Lambda\geq 32.6$ Å (not shown). At $\Lambda=26.0$ Å a noticeable broadening of the Bragg peak is accompanied by diminished satellite intensities, and at $\Lambda\leq 24.8$ Å the structure breaks down completely, as in the $\Lambda=12.5$ Å spectrum in Fig. 6. The perpendicular structural coherence length, as determined from the FWHM of the Bragg peak, is approximately constant at 200 Å for $\Lambda\geq 32$ Å, which is slightly better than the undoped films. For these 15 at. % Al–doped films the structural breakdown, which occurs at $\Lambda\approx 25$ Å, is higher than the 16.6 Å observed in the undoped films.[4] In contrast, we found that films containing approximately 20–25 at. % Al show only the single, broad, amorphouslike peak with no satellites for all Λ up to approximately 150 Å, indicating no superlattice structure exists over this wavelength range.

Second-order superlattice peaks around the Ni(222) and Mo(220) refections are very easily detected in the 15 at. % Al–doped samples for $\Lambda\geq 32$ Å. The modulation wavelengths and the average d spacings calculated from these second-order peaks show excellent agreement with the first-order reflections.

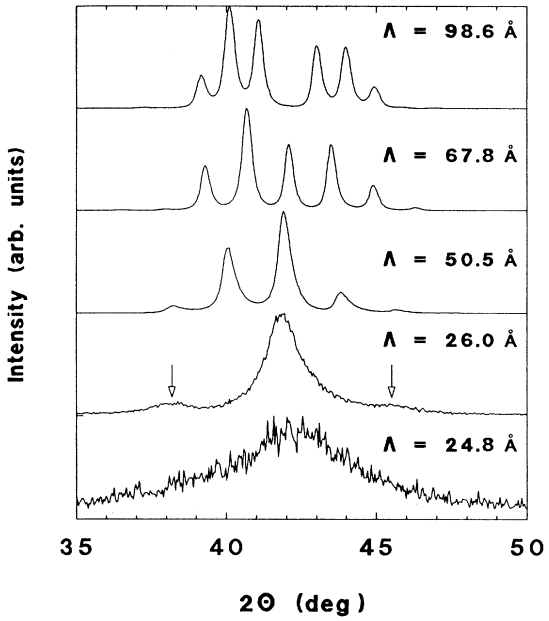

FIG. 7. High-angle x-ray-diffraction spectra for a series of Mo/Ni superlattices doped with 15 at. % Al.

To characterize the change in the composition profile of the doped Mo/Ni films, we analyzed the Bragg and satellite peak intensities of the first-order reflections, as satellite peak intensities give information on the composition wave of superlattices.[20] After the Lorentz, polarization, and absorption factors were divided out, the intensities were normalized to the total sum of intensities of each reflection manifold. The normalized intensities of each order satellite were plotted as a function of Λ for both the undoped and the 15 at. % Al–doped films, where the peaks analyzed include the Bragg peak and the first- and second-order satellites at both higher and lower 2θ. We find that for each of the five peaks included in this analysis the intensity-versus-Λ behavior is the same for both the doped and undoped films. As a further comparison we plotted the results of a similar analysis on the Mo/Ni samples reported in Ref. 4 and found very good agreement with the intensities from our study. Therefore, we conclude that the effects of an overall 15 at. % Al dopant level on the superlattice structure of Mo/Ni are small, as detected by high-angle x-ray diffraction.

The average perpendicular lattice spacings were calculated from the Bragg-peak positions and were found to correlate with the surface-wave velocities for both the undoped and 15 at. % Al–doped samples. However, no systematic strain differences were detected in the doped films. A correlation of lattice strain to surface-wave velocity has been found previously in Mo/Ni, where the elastic changes were attributed to changes in the Ni lattice.[4,6] Elastic phenomena have been correlated to lattice strain in several other metal-metal multilayered systems.[21,22]

Low-angle x-ray scattering was used to check the periodicity of the multilayers and to give qualitative information on the composition modulation of the films. Because of the geometry of the diffractometer used for these measurements, the intensities of the low-angle peaks cannot be taken as absolute, and only qualitative information can be obtained on the composition modulation of the films. In the low-angle spectra of the undoped Mo/Ni the odd-order peaks are very intense relative to the even-order peaks, where the absence of even-order peaks is expected in Mo/Ni and indicates square-wave composition modulation.[4] In contrast, in the low-angle spectra of the films doped with 15–25 at. % Al the even-order peaks are slightly more intense, indicating qualitatively that the square-wave composition modulation in the growth direction is replaced by a slightly more sinusoidal modulation. This could be the result of an Al concentration gradient in the Ni layers.

The modulation wavelengths of the superlattices were calculated from the high-angle satellite peak positions.[18] In the low-angle spectra, peak shifts caused by geometric factors are expected to decrease with increasing 2θ,[23] and the positions of the mth reflections are expected to represent the actual Λ at higher 2θ. We find empirically that for the undoped superlattices demonstrating high-angle satellites the values of Λ determined from the mth low-angle reflections occurring at 2θ greater than approximately 6° agree to within $\sim 1\%$ with those determined from the high-angle satellites. Therefore, for the multilayers with no high-angle satellite peaks, we calculated Λ using their mth low-angle peak positions occurring at $2\theta > 6°$, and no extrapolation method was used to find Λ.

VI. DISCUSSIONS AND CONCLUSIONS

The results of the x-ray diffraction indicate that an average Al concentration of up to 15 at. % in Mo/Ni superlattices has very little effect on the superlattice structure. Also, the Auger chemical maps indicate that the Al is segregating from the Mo layers into the Ni layers, and the XPS results indicate no shifts in the Ni $2p$ peak. Fuggle *et al.*[24] have found very little difference in the XPS peak position and line shape of the Ni $3d_{5/2}$ peak of Ni_3Al compared to pure Ni, whereas noticeable changes in NiAl and $NiAl_3$ were observed. We believe that at average Al dopant levels up to approximately 25 at. % Ni_3Al is the predominant Ni-Al phase formed in the Ni layers.

Structurally the formation of Ni_3Al is favorable because it is an ordered intermetallic alloy with a fcc structure and a bulk lattice constant of 3.57 Å, very similar to the structure of Ni, which has a bulk lattice constant of 3.52 Å.[7] Also the formation of Ni_3Al is favorable for thermodynamic reasons because fcc Ni_3Al has a lower free energy than amorphous phases of Ni-Al,[25] so that an ordered phase is expected to form, and it has a more negative heat of formation than the Mo-rich molybdenum aluminides.[26]

Cantor and Cahn[27] have found that the degree of surface mobility during sputter deposition is sufficient for the formation of an ordered Ni_3Al phase. In a study on metastable phase formation in the Al-Ni and Al-Cu sys-

tems, these authors have calculated the mean surface diffusion distance per depositing atom during growth to be 100 Å, where a sample temperature of 295 K and a deposition rate of 2 Å/s were assumed. These conditions are within our present experimental parameters, and these results support our evidence that Ni_3Al forms within the Ni layers during the growth of the Al-doped Mo/Ni multilayers.

The diffusion of Al from the Mo to the Ni layers is presumably grain-boundary diffusion similar to that seen for the low-temperature (75–150 °C) diffusion of copper through gold.[28] The driving force for this diffusion is believed to be the chemical-potential gradient resulting from the bilayer modulation, as the Ni layers act as very strong Al sinks because of the heat of formation of the ordered Ni_3Al phase discussed above.

At dopant levels above approximately 15 at. % the Al begins to noticeably affect the structural properties of Mo/Ni, as seen in the x-ray-diffraction spectra for all Λ. For an overall average atomic concentration of 15% in the film if the Al migrates to the Ni layers, then the [Al]:[Ni] concentration ratio is approximately 0.35 (assuming that the Al completely segregates into the Ni layers). This is very close to the [Al]:[Ni] ratio in stoichiometric Ni_3Al. Therefore, in the 25 at. % Al–doped films the excess Al may be precipitating out as other Ni-Al phases, such as NiAl or $NiAl_3$, or oxidizing to form Al_2O_3 or $NiAl_2O_4$, none of which is structurally compatible with the Ni lattice. Even though the XPS scans do not show evidence of other Ni-Al phases, we do not rule out this possibility, as their concentrations may be below the XPS detection limit. Currently we are trying to understand what exactly this excess Al is doing. We have indications that in the Ni layers in both the 15 and 25 at. % Al-doped samples there are multiple regions of varying Ni-Al composition, as indicated by evidence in both the low- and high-angle x-ray spectra not discussed here. These findings are currently under further investigation and will be presented in a future publication.

Previous studies[29–31] on Ni/Al bilayers and multilayers have found $NiAl_3$ to be the initial phase formed at the interfaces, where elevated temperatures were usually required for significant amounts of this phase to form. Ruckman *et al.*[32] did a study of room-temperature reactions between Ni and Al and found again that the aluminum-rich $NiAl_3$ phase is formed. In all of these studies the availability of Al was plentiful, and it was determined that the diffusion of Al plays an important role in the formation of the Ni-Al phases. In our work presented here we find that the nickel-rich phase Ni_3Al forms at room temperature in the Ni layers of Mo/Ni multilayers in which Al is codeposited in both layers on an overall 15-at. % level. Our results also demonstrate that the diffusion of Al is significant in the formation of this Ni-Al phase. These films are aluminum poor, and at higher dopant levels we suspect the formation of other Ni-Al phases. In comparison to the previous studies mentioned above our results suggest that the availability of Al might dictate the phase of formation in room-temperature reactions between Ni and Al.

We have found that Al dopant levels up to approximately 15 at. % have very little effect on the structural properties of Mo/Ni, whereas dopant levels above this greatly affect the superlattice structure. We suspect that this is a result of the precipitation of Ni-Al phases other than Ni_3Al. In the films doped at the 15-at. % level we observed a structural breakdown occurring at $\Lambda \approx 25$ Å instead of at 16.6 Å, as observed previously[4] in undoped Mo/Ni films. This could be a result of low concentrations of incompatible Ni-Al phases, as the wavelength below which superlattices are unable to accommodate impurities increases with increasing impurity levels. The breakdown observed at 16.6 Å in the undoped Mo/Ni, as reported in Ref. 4, could be a result of the residual vacuum contaminants since those films were grown in the $\sim 1 \times 10^{-7}$-Torr range. We are currently growing Mo/Ni films under ultrahigh-vacuum conditions to see how much of an effect low concentrations of impurities, such as O and C, have on the structure of Mo/Ni at small Λ.

With the structural behavior of Al-doped Mo/Ni in mind, the elastic behavior of these films becomes more clear. In previous studies[4,6] the elastic effects in Mo/Ni were attributed to changes in the Ni lattice. In agreement with this we are finding that at Al dopant levels up to 15 at. % the effects on the structure of the Ni layers are minor, and there is only a small change from the elastic properties of the undoped films. This is consistent with the formation of Ni_3Al in the Ni layers because the bulk shear elastic constant of Ni_3Al ($c_{44} = 1.24 \times 10^{11}$ N/m^2)[33] is very similar to that of bulk Ni ($c_{44} = 1.22 \times 10^{11}$ N/m^2).[34] However, at dopant levels of 20–25 % a breakdown in the structure is coincident with the disappearance of the elastic softening anomaly that was observed for Λ below approximately 50 Å in the undoped and 15 at. %–doped films. It seems that an elastic "rehardening" is associated with the disappearance of good superlattice structure, as we have found in the Al-doped films and as Khan *et al.*[4] observed in undoped Mo/Ni for $\Lambda \leq 16$ Å.

In summary, we have demonstrated impurity effects in Mo/Ni superlattices induced by the presence of Al. These effects appear simultaneously in both the structural and elastic properties as determined respectively by x-ray-diffraction and SAW measurements. However, the effects are not noticeable at average Al concentrations of up to approximately 15 at. %, where AES indicates strong Al segregation into the Ni layers. The results from x-ray diffraction and XPS suggest the formation of Ni_3Al, in agreement with thermodynamics. At Al concentrations above ≈ 15 at. % the excess Al, most likely precipitated out as other Ni-Al alloy phases or oxidized Al, causes a structural breakdown in the Mo/Ni superlattices and a rehardening of an observed in the surface-wave velocity.

ACKNOWLEDGMENTS

Financial support through the U.S. Office of Naval Technology for J.L.M. is gratefully acknowledged. In addition, the authors greatly appreciate assistance from

Denis Webb at the Naval Research Laboratory (NRL) in the setup of the SAW technique. Furthermore, the authors thank Alan Edelstein, also of NRL, for the use of the vacuum-deposition system, and Greg Gillen of The National Institute of Standards and Technology for sputtering the craters used in the bevel-depth-profiling analysis. This work was supported in part by the U.S. Office of Naval Research.

[1]D. A. G. Bruggeman, Ann. Phys. (Leipzig) **29**, 160 (1937).
[2]See references in M. Grimsditch, Phys. Rev. B **33**, 3891 (1986).
[3]I. K. Schuller, in *IEEE Ultrasonics Symposia Proceedings 1986,* edited by B. R. McAvoy (IEEE, New York, 1986), p. 1093.
[4]M. R. Khan, C. S. L. Chun, G. P. Felcher, M. Grimsditch, A. Kueny, C. M. Falco, and I. K. Schuller, Phys. Rev. B **27**, 7186 (1983).
[5]J. L. Makous and C. M. Falco, Solid State Commun. **68**, 375 (1988).
[6]I. K. Schuller and A. Rahman, Phys. Rev. Lett. **50**, 1377 (1983).
[7]*A Handbook of Lattice Spacings and Structures of Metals and Alloys,* edited by W. B. Pearson (Pergamon, Oxford, 1967).
[8]R. Danner, R. P. Huebener, C. S. L. Chun, M. Grimsditch, and I. K. Schuller, Phys. Rev. B **33**, 3696 (1986).
[9]From *Microwave Acoustics Handbook, Vol. 2. Surface Wave Velocities,* edited by A. J. Slobodnik, Jr., R. T. Delmonico, and E. D. Conway (Air Force Cambridge Research Laboratories, Bedford, 1974).
[10]*Microwave Acoustics Handbook, Vol. 1. Surface Wave Velocities,* edited by A. J. Slobodnik, Jr. and E. D. Conway (Air Force Cambridge Research Laboratories, Bedford, 1970).
[11]W. R. Smith, H. M. Gerard, J. H. Collins, T. M. Reeder, and H. J. Shaw, IEEE Trans. Microwave Theory Tech. **MTT-17**, 865 (1969).
[12]H. F. Tiersten, J. Appl. Phys. **40**, 770 (1969).
[13]L. E. Davis, N. C. McDonald, P. W. Palmberg, G. E. Riach, and R. E. Weber, in *Handbook of Auger Electron Spectroscopy,* 2nd ed. (Physical Electronics Industries, Inc., Eden Prairie, MN, 1976).
[14]S. M. Hues, Mater. Sci. Eng. B **6**, 205 (1990).
[15]A. Zalar and S. Hoffman, Surf. Interface Anal. **2**, 183 (1980).
[16]C. D. Wagner, W. M. Riggs, L. E. Davis, J. F. Moulder, and G. E. Muilenberg, in *Handbook of X-Ray Photoelectron Spectroscopy,* edited by G. E. Muilenberg (Perkin-Elmer Corp., Eden Prairie, MN, 1979).
[17]V. I. Nefedov, J. Electron Spectrosc. Relat. Phenom. **25**, 29 (1982).
[18]I. K. Schuller, Phys. Rev. Lett. **44**, 1597 (1980).
[19]H. P. Klug and L. E. Alexander, in *X-Ray Diffraction Procedures,* 2nd ed. (Wiley, New York, 1974), Chap. 9.
[20]A. Segmüller and A. E. Blakeslee, J. Appl. Crystallogr. **6**, 19 (1973).
[21]J. L. Makous and C. M. Falco, Solid State Commun. **72**, 667 (1989).
[22]P. Bisanti, M. B. Brodsky, G. P. Felcher, M. Grimsditch, and L. R. Sill, Phys. Rev. B **35**, 7813 (1987).
[23]B. D. Cullity, *Elements of X-Ray Diffraction,* 2nd ed. (Addison-Wesley, Reading, MA, 1978), pp. 359–367.
[24]J. C. Fuggle, F. U. Hillebrecht, R. Zeller, Z. Zolnierek, P. Bennett, and C. Freiburg, Phys. Rev. B **27**, 2145 (1982).
[25]J. S. C. Jang and C. C. Koch, J. Mater. Res. **5**, 498 (1990).
[26]F. R. de Boer, R. Boom, W. C. M. Mattens, A. R. Miedema, and A. K. Niessen, *Cohesion in Metals: Transition Metal Alloys* (North-Holland, Amsterdam, 1989), pp. 309 and 416.
[27]B. Cantor and R. W. Cahn, Acta Metall. **24**, 845 (1976).
[28]H. G. Tompkins and M. R. Pinnel, J. Appl. Phys. **47**, 3804 (1976).
[29]E. G. Colgan, M. Nastasi, and J. W. Mayer, J. Appl. Phys. **58**, 4125 (1985).
[30]M. Nastasi, L. S. Hung, and J. W. Mayer, Appl. Phys. Lett. **43**, 831 (1983).
[31]E. Ma, C. V. Thompson, and L. A. Clevenger, J. Appl. Phys. **69**, 2211 (1991).
[32]M. W. Ruckman, L. Jiang, and M. Strongin, J. Vac. Sci. Technol. A **8**, 134 (1990).
[33]F. Wallow, G. Neite, W. Schröer, and E. Nembach, Phys. Status Solidi A **99**, 483 (1987).
[34]K. Salama and J. A. Alers, Phys. Status Solidi A **41**, 241 (1977).

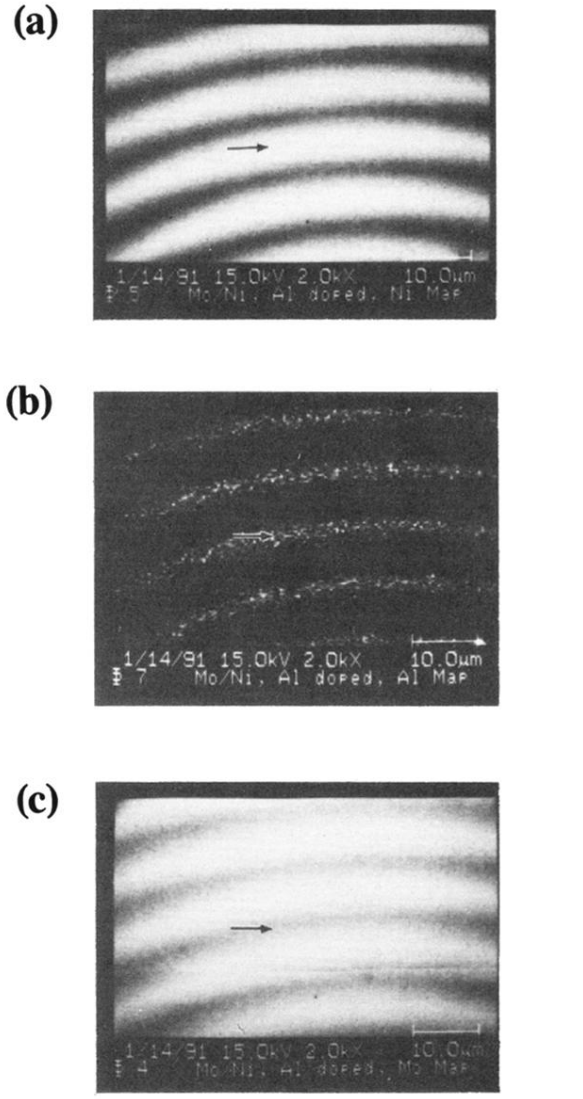

FIG. 5. AES compositional maps for (a) Ni, (b) Al, and (c) Mo in a $\Lambda = 98.6$ Å Mo/Ni superlattice doped with 15 at. % Al. Light regions correspond to where the element is detected, and the arrows indicate the same position on the sample.